Coastal Engineering 71 (2013) 52–59

Contents lists available at SciVerse ScienceDirect

Coastal Engineering

journal homepage: www.elsevier.com/locate/coastaleng

Decomposition of incident and reflected surface waves using an Ultrasonic Velocity Profiler

Rodrigo Mosquera *, Francisco Pedocchi

Instituto de Mecánica de los Fluidos e Ingeniería Ambiental, Facultad de Ingeniería, Universidad de la República, Julio Herrera y Reissig 565, Uruguay

ARTICLE INFO

Article history:
Received 11 April 2012
Received in revised form 5 August 2012
Accepted 9 August 2012
Available online xxxx

Keywords:
Ultrasonic Velocity Profiler
Incident and reflected waves
Wave flume

ABSTRACT

In this article a novel method for estimating incident and reflected waves in wave flumes is presented. Instead of using water surface measurements obtained with a series of wave gages, we used water velocity measurements inside the water column obtained with an Ultrasonic Velocity Profiler to decompose the wave field. The technique allows for the identification of the incident and reflected first harmonic waves and the incident and reflected free and bound second harmonic waves. Only velocity measurements over a small fraction of the first harmonic wavelength are necessary to obtain reliable results, making the method suitable for studies where the water depth is not constant. Wave measurements obtained in a wave flume using four wave gages and three levels of wave reflection are used to evaluate the new method with excellent results. Finally, since no calibration of the velocity profiler is necessary, it is foreseen that the method could be implemented in a stand-alone instrument that would give the user the wave field decomposition without the need of a case by case set-up and calibration.

1. Introduction

Understanding the transformation of waves when they are reflected on the sea coast or on sea structures is of obvious relevance for coastal engineering. For example, after a new structure is placed in a harbor, the interaction among incident and reflected waves can produce important modifications to the wave field affecting the harbor agitation. Regarding coastal morphodynamics, when modifications are introduced on the coast, the interaction between incident and reflected waves modifies the velocities in the water column and close to the seabed, impacting on sediment transport and beach morphology. In the hydraulic laboratory, correctly characterizing incident and reflected waves is critical for the study of wave–structure interactions and for the study of nonlinear interactions among different components of the wave field.

In laboratory flumes, waves are usually generated using a wave maker. The boundary condition imposed on the water motion on the wave maker results on the generation of not only a primary wave but also several secondary waves with different celerities. This obscures the interpretation of laboratory observations as noted by Madsen (1971). Madsen (1971) used a second order wave theory to show that a piston type wave maker with a purely sinusoidal motion would generate, on top of a first harmonic wave, two second harmonic waves: a Stokes second order progressive wave and a bound wave, which is generally longer and faster than the second harmonic Stokes' wave. The presence of waves with the same frequency but different wavelength results on the amplitude modulation of the second harmonic along the wave flume. The same could be expected for the third and higher harmonics. However, in experiments with regular waves these harmonics tend to contain relatively low energy. The presence of both a free and a bound second harmonic wave adds additional complexity to the study of the wave reflection as has been recently reported in the literature (Hancock, 2005; Lin and Huang, 2004).

There are different methods for the decomposition of incident and reflected waves in wave flumes using water surface measurements. The most popular ones are the methods developed by Goda and Suzuki (1976) and by Mansard and Funke (1980). Both methods allow for the study of the reflection of regular and irregular waves. Goda and Suzuki (1976) proposed a technique to estimate the incident and reflected waves from the simultaneous records of two wave gages located along the flume. Later Mansard and Funke (1980) proposed a least square method to separate incident and reflected waves using simultaneous measurements with three wave gages. Mansard and Funke's (1980) method overcomes several of the limitations of Goda and Suzuki's (1976) method. However, as it was the case of Goda and Suzuki's (1976) method Mansard and Funke (1980) also does not takes into account the presence of free and locked modes in the higher harmonics. Recently, Lin and Huang (2004) proposed a method for estimating both incident and reflected waves that differentiate free and locked modes in the higher harmonics. Lin and Huang's (2004) method uses simultaneous measurements at four wave gages to obtain the incident and reflected first harmonics, and the free and locked modes of the incident and reflected second harmonics.

* Corresponding author.
E-mail addresses: rmosquer@fing.edu.uy (R. Mosquera), kiko@fing.edu.uy (F. Pedocchi).

0378-3839/$ – see front matter © 2012 Elsevier B.V. All rights reserved.
http://dx.doi.org/10.1016/j.coastaleng.2012.08.002

A different path was taken by Hughes (1993) who proposed a method using co-located gages (a conventional wave gage and a laser Doppler velocimeter). Hughes (1993) method does not account for the presence of free and locked modes. However, it was the first laboratory method that moved the focus away from the measurement of the water surface elevation and into the measurement of the velocity field inside the water column. From the time of publication of Hughes (1993) work, the field of hydro-acoustics has experienced an extremely fast growth, and acoustic velocity meters of different kinds are now available at most hydraulic laboratories, making Hughes work even more relevant than it was at the time of its publication.

In this work, we describe a novel method to decompose the incident and reflected waves of a regular wave field generated inside a wave flume, characterizing both free and bound second harmonic waves. The technique uses the velocity measurements inside the water column obtained with an Ultrasonic Velocity Profiler — UVP (Met-Flow, 2002; Pedocchi and García, in press). However, it can be adapted to any other device that is able to simultaneously record water velocities in several points along the water column. The UVP measures the projection of the water velocity over an axis aligned with the sensor, as sketched in Fig. 1; further details of the experimental set up are given in Section 3.

The theoretical background of the proposed technique can be traced back to the works of Mansard and Funke (1980), Hughes (1993), and Lin and Huang (2004), but it presents several particularities which are discussed in detail in Section 2. The implementation of the theory to the particular case of the UVP is presented in Section 3. In Section 4 the results obtained applying the technique to three wave reflection scenarios measured in a laboratory wave flume are shown. The considered scenarios were: very low reflection, complete reflection, and partial reflection. The results obtained with the new technique are compared with the ones obtained using simultaneous surface elevation measurements from four wave gages and applying the method described by Lin and Huang (2004). This also serves as an experimental validation for the Lin and Huang's (2004) method, which was originally only validated with synthetic signals. Finally, to close this article, some advantages of the proposed method over the existing ones are discussed and several extensions to the method for more complex situations are outlined.

2. Theory

Havelock (1929) proposed a general theory for the mechanical generation of waves. Later, Biesel and Suquet (1951) made several contributions on both the theoretical and practical aspects of the wave generation using piston-type and flap-type wavemakers. Fontanet (1961) developed a complete second order theory in Lagrangian coordinates for the wave field generated by a sinusoidally moving wave maker. Madsen (1971) developed an approximation to a second-order wave maker theory in Eulerian coordinates assuming relatively long waves generated by a piston-type wave maker. Sulisz and Hudspeth (1993) extended Madsen's work to a complete second-order solution for water waves generated by a generic-type wave maker.

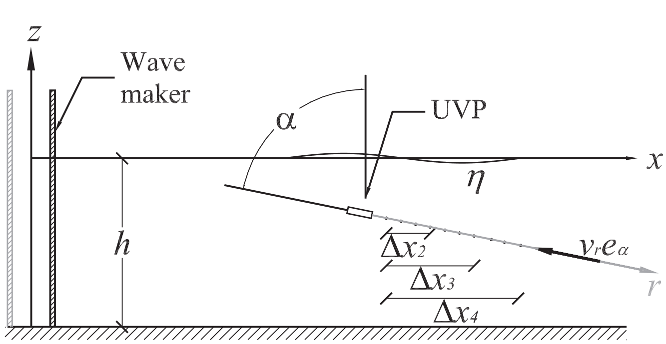

Fig. 1. Scheme showing the UVP set-up. The main variables and the distances among the four measuring points (channels) used for the wave field characterization are indicated.

The second-order wave maker theory has shown to be a useful analytical solution, presenting very good agreement with experiments (Hancock, 2005; Madsen, 1971; Sulisz and Hudspeth, 1993). The main outcome of this theory is the prediction of two second harmonic waves: A bounded second harmonic progressive wave (phase-locked mode), with the same celerity as the first harmonic. And a free wave (free mode), with its celerity given by the dispersion equation. This free mode may be canceled out if a second harmonic movement is added to the wave maker motion. The complete solution predicts additional terms that reflect the fact that the motion of the wave maker does not correspond exactly to the motion that the water particles would have according to the second order wave theory. These terms are called evanescent modes and they decay exponentially with x away from the wave maker. Sulisz and Hudspeth (1993) predict that the evanescent modes at $x>3h$ are less than 1% of their original value at $x=0$.

Following the notation of Madsen (1971), the water surface associated with a progressive wave generated by a piston type wave maker in a wave flume may be expressed to the second order as (Fig. 1)

$$\begin{aligned}\eta &= \eta^{(1)}+\eta^{(2)} = \eta^{(1)}+\eta_B^{(2)}+\eta_F^{(2)} \\ &= -a^{(1)}sin(k_0x-\omega t)-a_B^{(2)}cos2(k_0x-\omega t)+a_F^{(2)}cos(\kappa x-2\omega t+\delta),\end{aligned} \tag{1}$$

where $\eta^{(1)}$ is the first order solution, $\eta_B^{(2)}$ is the second order solution that satisfies the inhomogeneous boundary condition at $y=0$ disregarding the boundary condition at the wave maker (bound wave), and $\eta_F^{(2)}$ is the second order solution that satisfies the homogeneous linearized equations and the boundary condition at the wave maker (free mode), δ is the phase shift of the second-order free mode. The waves numbers k_0 and κ are obtained from the corresponding dispersion equations

$$\omega^2 = k_0 g tanh(k_0 h), \tag{2}$$

$$(2\omega)^2 = \kappa g tanh(\kappa h), \tag{3}$$

with ω the angular frequency of the fundamental period, g the gravitational acceleration, and h the water depth.

The velocity potential ϕ expanded to the second order is

$$\phi = \phi^{(1)}+\phi^{(2)}+O\left(\epsilon^3\right), \tag{4}$$

where $\phi^{(1)}$ and $\phi^{(2)}$ are the first-order and second order solutions of the velocity potential, respectively, $O(\ ^3)$ is a term of order $\ ^3$, and   is a small quantity equal to $a^{(1)}k_0$. Following Eq. (1), $\phi^{(2)}$ may be expressed as the sum of $\phi_B^{(2)}$ and $\phi_F^{(2)}$. With $\phi_B^{(2)}$ taken to satisfy the inhomogeneous boundary condition at $z=0$, disregarding the boundary condition at the wave maker, and $\phi_F^{(2)}$ taken to satisfy the homogeneous, linearized equations and the boundary condition at the wave maker.

Assuming that both incident and reflected waves exist into the flume, each of above potentials may be expressed as

$$\begin{aligned}\phi^{(1)} &= a_I^{(1)}Z^{(1)}cos\left[k_0x-\omega t+\delta_I^{(1)}\right]-a_R^{(1)}Z^{(1)}cos\left[k_0x+\omega t+\delta_R^{(1)}\right], \\ \phi_B^{(2)} &= -a_{I,B}^{(2)}Z_B^{(2)}sin\left[2(k_0x-\omega t)+\delta_{I,B}^{(2)}\right]+a_{R,B}^{(2)}Z_B^{(2)}sin[2(k_0x+\omega t)+\ldots\end{aligned} \tag{5}$$

$$\ldots+\delta_{R,B}^{(2)}]+b_t(t)+b_x(x), \tag{6}$$

$$\phi_F^{(2)} = a_{I,F}^{(2)}Z_F^{(2)}sin\left[\kappa x-2\omega t+\delta_{I,F}^{(2)}\right]-a_{R,F}^{(2)}Z_F^{(2)}sin\left[\kappa x+2\omega t+\delta_{R,F}^{(2)}\right], \tag{7}$$

with

$$Z^{(1)} = \frac{g\,cosh[k_0(h+z)]}{\omega\,cosh(k_0 h)}, \tag{8}$$

$$Z_B^{(2)} = \frac{g\,cosh[2k_0(h+z)]}{2\omega\,cosh(2k_0 h)}, \tag{9}$$

$$Z_F^{(2)} = \frac{g\,cosh[\kappa(h+z)]}{2\omega\,cosh(\kappa h)}. \tag{10}$$

Where a is the amplitude, the subscripts $_I$ and $_R$ indicate incident and reflected waves, the subscripts $_B$ and $_F$ indicate locked and free modes, the superscript $^{(n)}$ denotes the n^{th} harmonic wave, δ is the phase from an arbitrary time origin, $b_x(x)$ and $b_t(t)$ are functions that group non-progressive waves resulting from the application of a second-order wave theory.

Even though Madsen's (1971) theory allows for the determination of the phase shift among the different incident harmonics, the interaction among the reflected waves and the wave maker is not considered in this theory. Therefore the phases of the different waves are considered to be unknown in the mathematical manipulations that follow.

Imposing the dynamic boundary condition at the free surface gives

$$\eta^{(1)} = -\frac{1}{g}\frac{\partial\phi^{(1)}}{\partial t}, \tag{11}$$

$$\eta^{(2)} = -\frac{1}{g}\frac{\partial\phi^{(2)}}{\partial t} - \frac{1}{g}\left[\frac{1}{2}\left(\frac{\partial\phi^{(1)2}}{\partial x} + \frac{\partial\phi^{(1)2}}{\partial z}\right) + \frac{\partial^2\phi^{(1)}}{\partial t\partial z}\eta^{(1)}\right]. \tag{12}$$

After some algebraic manipulations and discarding the non-progressive terms, the boundary condition at the free surface gives

$$\begin{aligned}\eta^{(1)}+\eta^{(2)} = &-a_I^{(1)} sin\left[k_0x-\omega t+\delta_I^{(1)}\right] - a_R^{(1)} sin\left[k_0x+\omega t+\delta_R^{(1)}\right] - \ldots\\ &\ldots - a_{I,B}^{(2)} cos\left[2(k_0x-\omega t)+\delta_{I,B}^{(2)}\right] + a_I^{(1-2)} cos\left[2\left(k_0x-\omega t+\delta_I^{(1)}\right)\right] - \ldots\\ &\ldots - a_{R,B}^{(2)} cos\left[2(k_0x+\omega t)+\delta_{R,B}^{(2)}\right] + a_R^{(1-2)} cos\left[2\left(k_0x+\omega t+\delta_R^{(1)}\right)\right] + \ldots\\ &\ldots + a_{I,F}^{(2)} cos\left[\kappa x-2\omega t+\delta_{I,F}^{(2)}\right] + a_{R,F}^{(2)} cos\left[\kappa x+2\omega t+\delta_{R,F}^{(2)}\right].\end{aligned} \tag{13}$$

Note that two terms with frequency 2ω appear on Eq. (13) as a result of the last three non linear terms in Eq. (12). Their amplitudes are given by

$$a_I^{(1-2)} = \frac{a_I^{(1)2} k_0}{4}\frac{\left[1-3tanh^2(k_0h)\right]}{tanh(k_0h)}, \tag{14}$$

$$a_R^{(1-2)} = \frac{a_R^{(1)2} k_0}{4}\frac{\left[1-3tanh^2(k_0h)\right]}{tanh(k_0h)}. \tag{15}$$

These amplitudes are functions of the first harmonic amplitudes and are of second order. These terms are of the same form as the ones derived from the second order locked modes of the velocity potential, and can be grouped with them defining the amplitude of the new bounded surface modes, each of them with their corresponding amplitude b and phase φ

$$\begin{aligned}b_{I,B}^{(2)} cos\left[2(k_0x-\omega t)+\varphi_{I,B}^{(2)}\right] = &-a_{I,B}^{(2)} cos\left[2(k_0x-\omega t)+\delta_{I,B}^{(2)}\right] + \ldots\\ &+a_I^{(1-2)} cos\left[2\left(k_0x-\omega t+\delta_I^{(1)}\right)\right],\end{aligned} \tag{16}$$

$$\begin{aligned}b_{R,B}^{(2)} cos\left[2(k_0x-\omega t)+\varphi_{R,B}^{(2)}\right] = &-a_{R,B}^{(2)} cos\left[2(k_0x-\omega t)+\delta_{R,B}^{(2)}\right] + \ldots\\ &+a_R^{(1-2)} cos\left[2\left(k_0x-\omega t+\delta_R^{(1)}\right)\right].\end{aligned} \tag{17}$$

The free surface can therefore be expressed as

$$\begin{aligned}\eta^{(1)}+\eta^{(2)} = &-a_I^{(1)} sin\left[k_0x-\omega t+\delta_I^{(1)}\right] - a_R^{(1)} sin\left[k_0x+\omega t+\delta_R^{(1)}\right] - \ldots\\ &\ldots + b_{I,B}^{(2)} cos\left[2(k_0x-\omega t)+\varphi_{I,B}^{(2)}\right] + b_{R,B}^{(2)} cos\left[2(k_0x+\omega t)+\varphi_{R,B}^{(2)}\right] + \ldots\\ &\ldots + a_{I,F}^{(2)} cos\left[\kappa x-2\omega t+\delta_{I,F}^{(2)}\right] + a_{R,F}^{(2)} cos\left[\kappa x+2\omega t+\delta_{R,F}^{(2)}\right].\end{aligned} \tag{18}$$

As Eqs. (16) and (17) show, for the particular case of the second order wave theory the non-linear interactions contribute to the free surface adding terms of the same form of the second order locked modes. Eq. (13) shows how these interactions should be considered when the velocity field is measured but the free surface level is required, for example when comparing the proposed method with the one of Lin and Huang (2004).

The horizontal and vertical velocities up to the second order can be computed respectively as

$$u^{(1)} + u^{(2)} = \frac{\partial\phi^{(1)}}{\partial x} + \frac{\partial\phi^{(2)}}{\partial x}, \tag{19}$$

$$w^{(1)} + w^{(2)} = \frac{\partial\phi^{(1)}}{\partial z} + \frac{\partial\phi^{(2)}}{\partial z}. \tag{20}$$

The UVP measures the projection of the velocity over an axis aligned with the sensor $\mathbf{e}_\alpha$ or radial velocity v_r, as sketched in Fig. 1. Therefore the radial velocity recorded with the UVP at an arbitrary point in space is given by

$$\begin{aligned}v_r(x,z,t) = \nabla\phi.\mathbf{e}_\alpha &= -u\,sin(\alpha) + w cos(\alpha) =\\ &= a_I^{(1)} k_0 \begin{bmatrix} Z^{(1)} sin\left(k_0x-\omega t+\delta_I^{(1)}\right) sin(\alpha) + \ldots (21)\\ \ldots + Y^{(1)} cos\left(k_0x-\omega t+\delta_I^{(1)}\right) cos(\alpha)\end{bmatrix} - \ldots\\ &\ldots - a_R^{(1)} k_0 \begin{bmatrix} Z^{(1)} sin\left(k_0x+\omega t+\delta_R^{(1)}\right) sin(\alpha) + \ldots (22)\\ \ldots + Y^{(1)} cos\left(k_0x+\omega t+\delta_R^{(1)}\right) cos(\alpha)\end{bmatrix} - \ldots\\ &\ldots - a_{I,B}^{(2)} 2k_0 \begin{bmatrix} -Z_B^{(2)} cos\left(2(k_0x-\omega t)+\delta_{I,B}^{(2)}\right) sin(\alpha) + \ldots (23)\\ \ldots + Y_B^{(2)} sin\left(2(k_0x-\omega t)+\delta_{I,B}^{(2)}\right) cos(\alpha)\end{bmatrix} + \ldots\\ &\ldots + a_{R,B}^{(2)} 2k_0 \begin{bmatrix} -Z_B^{(2)} cos\left(2(k_0x+\omega t)+\delta_{R,B}^{(2)}\right) sin(\alpha) + \ldots (24)\\ \ldots + Y_B^{(2)} sin\left(2(k_0x+\omega t)+\delta_{R,B}^{(2)}\right) cos(\alpha)\end{bmatrix} + \ldots\\ &\ldots + a_{I,F}^{(2)} \kappa \begin{bmatrix} -Z_F^{(2)} cos\left(\kappa x-2\omega t+\delta_{I,F}^{(2)}\right) sin(\alpha) + \ldots (25)\\ \ldots + Y_F^{(2)} sin\left(\kappa x-2\omega t+\delta_{I,F}^{(2)}\right) cos(\alpha)\end{bmatrix} - \ldots\\ &\ldots - a_{R,F}^{(2)} \kappa \begin{bmatrix} -Z_F^{(2)} cos\left(\kappa x+2\omega t+\delta_{R,F}^{(2)}\right) sin(\alpha) + \ldots (26)\\ \ldots + Y_F^{(2)} sin\left(\kappa x+2\omega t+\delta_{R,F}^{(2)}\right) cos(\alpha)\end{bmatrix} + e(x,z,t),\end{aligned} \tag{21}$$

with

$$Y^{(1)} = \frac{gs\,inh[k_0(h+z)]}{\omega cosh(k_0h)}, \tag{22}$$

$$Y_B^{(2)} = \frac{g\,sinh[2k_0(h+z)]}{2\omega cosh(2k_0h)}, \tag{23}$$

$$Y_F^{(2)} = \frac{g\,sinh[\kappa(h+z)]}{2\omega cosh(\kappa h)}, \tag{24}$$

and $e(x,z,t)$ a residual resulting from truncating the velocity potential expansion at the second order. This residual would in general not be zero for a measured signal.

The Fourier transform of the radial velocity is

$$\hat{v}_r^{(n)}(x,z) = \hat{v}_r(x,z,n\omega) = \frac{\omega}{2\pi}\int_0^{(2\pi/\omega)} v_r(x,z,t) exp(-in\omega t)dt. \tag{25}$$

To determine the incident and reflected first harmonic components measured at a location (x_m,z_m) the expression for $v_r^{(1)}$ given in Eq. (21) can be inserted in Eq. (25) with $n=1$ to obtain

$$\hat{v}_r^{(1)}(x_m, z_m) = C_I^{(1)}X_I^{(1)} + C_R^{(1)}X_R^{(1)} + \Omega_m^{(1)}, \tag{26}$$

where

$$X_I^{(1)} = a_I^{(1)} exp\left[-i\left(k_0x_1 + \delta_I^{(1)}\right)\right], \tag{27}$$

$$X_R^{(1)} = a_R^{(1)} exp\left[i\left(k_0x_1 + \delta_R^{(1)}\right)\right], \tag{28}$$

$$C_I^{(1)} = k_0\left[iZ^{(1)}sin(\alpha) + Y^{(1)}cos(\alpha)\right]exp[-i(k_0\Delta x_m)]/2, \tag{29}$$

$$C_R^{(1)} = k_0\left[iZ^{(1)}sin(\alpha) - Y^{(1)}cos(\alpha)\right]exp[+i(k_0\Delta x_m)]/2, \tag{30}$$

with $\Omega_m^{(1)}$ the Fourier transform of $e(x,z,t)$ for $n=1$ and Δx_m the horizontal distance to the first measured velocity point. Note that $Z^{(1)}$ and $Y^{(1)}$ are functions of z_m.

The optimal solutions for the complex numbers $X_I^{(1)}$ and $X_R^{(1)}$ are the ones that minimize the difference between the first harmonics of the measured signal for all the measuring locations. This optimal solution is obtained when the complex residual $\Omega_m^{(1)}$ is minimized in some sense over all measuring locations. Here the sum of the square of the amplitude of $\Omega_m^{(1)}$ for all m points is selected as the total residual to be minimized.

$$\sum_m \left|\Omega_m^{(1)}\right|^2 = \sum_m \Omega_m^{(1)}\Omega_m^{(1)*} = \sum_m \left|\hat{v}_r(x_m, z_m) - C_I^{(1)}X_I^{(1)} - C_R^{(1)}X_R^{(1)}\right|^2, \tag{31}$$

where the superscript * indicates complex conjugate and the straight brackets || complex norm.

Baquerizo Azofra (1995) pointed out that residual used by Mansard and Funke (1980) was a complex number. The minimization of this complex residual is therefore not formally possible, since complex numbers cannot be ordered. This problem was also found in the work of Lin and Huang (2004). Here the residual defined by Eq. (31) is a real number, and therefore it is possible to find a minimum. The residual would be minimum if $X_I^{(1)}$ and $X_R^{(1)}$ are selected such that

$$\frac{\partial \sum_m |\Omega_m^{(1)}|^2}{\partial X_I^{(1)*}} = \frac{\partial \sum_m |\Omega_m^{(1)}|^2}{\partial X_R^{(1)*}} = 0. \tag{32}$$

Here the definition of the partial derivative of a real valued function of complex variables introduced by Brandwood (1983) is used. Noting that $-C_I^{(1)*} = C_R^{(1)}$, the above expression gives

$$A^{(1)}X^{(1)} = b^{(1)}, \tag{33}$$

with

$$A^{(1)} = \begin{bmatrix} |C_I^{(1)}|^2 & -C_I^{(1)*2}(40) \\ -C_I^{(1)2} & |C_I^{(1)}|^2 \end{bmatrix}, \tag{34}$$

$$X^{(1)} = \begin{bmatrix} X_I^{(1)}(42) \\ X_R^{(1)} \end{bmatrix}, \tag{35}$$

$$b^{(1)} = \begin{bmatrix} C_I^{(1)*}\hat{v}_r(x_m, z_m)(44) \\ -C_I^{(1)}\hat{v}_r(x_m, z_m) \end{bmatrix}. \tag{36}$$

Finally, the first harmonics' amplitudes are computed as

$$a_I^{(1)} = |X_I^{(1)}|, \tag{37}$$

$$a_R^{(1)} = |X_R^{(1)}|. \tag{38}$$

The same procedure is applied for the computation of the second harmonic components

$$\hat{v}_r^{(2)}(x_m, z_m) = C_{I,B}^{(2)}X_{I,B}^{(2)} + C_{R,B}^{(2)}X_{R,B}^{(2)} + C_{I,F}^{(2)}X_{I,F}^{(2)} + C_{R,F}^{(2)}X_{R,F}^{(2)} + \Omega_m^{(2)}, \tag{39}$$

with

$$X_{I,B}^{(2)} = a_{I,B}^{(2)} exp\left[-i\left(2k_0x_1 + \delta_{I,B}^{(2)}\right)\right], \tag{40}$$

$$X_{R,B}^{(2)} = a_{R,B}^{(2)} exp\left[i\left(2k_0x_1 + \delta_{R,B}^{(2)}\right)\right], \tag{41}$$

$$X_{I,F}^{(2)} = a_{I,F}^{(2)} exp\left[-i\left(\kappa x_1 + \delta_{I,F}^{(2)}\right)\right], \tag{42}$$

$$X_{R,F}^{(2)} = a_{R,F}^{(2)} exp\left[i\left(\kappa x_1 + \delta_{R,F}^{(2)}\right)\right], \tag{43}$$

$$C_{I,B}^{(2)} = +2k_0\left[Z_B^{(2)}sin(\alpha) - iY_B^{(2)}cos(\alpha)\right]exp(-i(2k_0\Delta x_m))/2, \tag{44}$$

$$C_{R,B}^{(2)} = -2k_0\left[Z_B^{(2)}sin(\alpha) + iY_B^{(2)}cos(\alpha)\right]exp(+i(2k_0\Delta x_m))/2, \tag{45}$$

$$C_{I,F}^{(2)} = -\kappa\left[Z_F^{(2)}sin(\alpha) - iY_F^{(2)}cos(\alpha)\right]exp(-i(\kappa\Delta x_m))/2, \tag{46}$$

$$C_{R,F}^{(2)} = +\kappa\left[Z_F^{(2)}sin(\alpha) + iY_F^{(2)}cos(\alpha)\right]exp(+i(\kappa\Delta x_m))/2. \tag{47}$$

and $\Omega_m^{(2)}$ the Fourier transform of $e(x,z,t)$ for $n=2$.

As it was done with the first harmonic the sum of the square of the amplitude of $\Omega_m^{(2)}$ for all m points is selected as the total residual to be minimized.

$$\frac{\partial \sum_m |\Omega_m^{(2)}|^2}{\partial X_{I,B}^{(2)*}} = \frac{\partial \sum_m |\Omega_m^{(2)}|^2}{\partial X_{R,B}^{(2)*}} = \frac{\partial \sum_m |\Omega_m^{(2)}|^2}{\partial X_{I,F}^{(2)*}} = \frac{\partial \sum_m |\Omega_m^{(2)}|^2}{\partial X_{R,F}^{(2)*}} = 0. \tag{48}$$

Noting that $-C_{I,B}^{(2)*} = C_{R,B}^{(2)}$ and $-C_{I,F}^{(2)*} = C_{R,F}^{(2)}$, solving the above expression is equivalent to solve

$$A^{(2)}X^{(2)} = b^{(2)}, \tag{49}$$

with

$$A^{(2)} = \begin{bmatrix} |C_{I,B}^{(2)}|^2 & -C_{I,B}^{(2)*2} & C_{I,B}^{(2)*}C_{I,F}^{(2)} & -C_{I,B}^{(2)*}C_{I,F}^{(2)*}(59) \\ -C_{I,B}^{(2)2} & |C_{I,B}^{(2)}|^2 & -C_{I,B}^{(2)}C_{I,F}^{(2)} & C_{I,B}^{(2)}C_{I,F}^{(2)*}(60) \\ C_{I,F}^{(2)*}C_{I,B}^{(2)} & -C_{I,F}^{(2)*}C_{I,B}^{(2)*} & |C_{I,F}^{(2)}|^2 & -C_{I,F}^{(2)*2}(61) \\ -C_{I,F}^{(2)}C_{I,B}^{(2)} & C_{I,B}^{(2)*}C_{I,F}^{(2)} & -C_{I,F}^{(2)2} & |C_{I,F}^{(2)}|^2 \end{bmatrix}, \tag{50}$$

$$X^{(2)} = \begin{bmatrix} X_{I,B}^{(2)}(63) \\ X_{R,B}^{(2)}(64) \\ X_{I,F}^{(2)}(65) \\ X_{R,F}^{(2)} \end{bmatrix}, \tag{51}$$

$$b^{(2)} = \begin{bmatrix} C_{I,B}^{(2)*}\hat{v}_r(x_m,z_m)(67) \\ -C_{I,B}^{(2)}\hat{v}_r(x_m,z_m)(68) \\ C_{I,F}^{(2)*}\hat{v}_r(x_m,z_m)(69) \\ -C_{I,F}^{(2)}\hat{v}_r(x_m,z_m) \end{bmatrix}. \quad (52)$$

Finally, the amplitudes of each of the second harmonics are

$$a_{I,B}^{(2)} = |X_{I,B}^{(2)}|, \quad (53)$$

$$a_{R,B}^{(2)} = |X_{R,B}^{(2)}|, \quad (54)$$

$$b_{I,B}^{(2)} = \left| -X_{I,B}^{(2)} + X_I^{(1)2}\frac{k_0}{4}\frac{\left[1-3tanh^2(k_0h)\right]}{tanh(k_0h)} \right|, \quad (55)$$

$$b_{R,B}^{(2)} = \left| -X_{R,B}^{(2)} + X_R^{(1)2}\frac{k_0}{4}\frac{\left[1-3tanh^2(k_0h)\right]}{tanh(k_0h)} \right|, \quad (56)$$

$$a_{I,F}^{(2)} = |X_{I,F}^{(2)}|, \quad (57)$$

$$a_{R,F}^{(2)} = |X_{R,F}^{(2)}|. \quad (58)$$

3. Implementation

3.1. Matrix condition

As reported by Lin and Huang (2004), Eq. (49) becomes singular when the determinant of the matrix $A^{(2)}$ equals zero. However, as early noted by Goda and Suzuki (1976) (in terms of wave gage spacings and wavelengths) there should be a divergence zone (or zone of high inaccuracy) adjacent to the singularity of Eq. (49). In terms of the described methodology, this divergence zone is associated with the condition of the matrix $A^{(2)}$. When $A^{(2)}$ becomes ill conditioned, solving system (49) without taking the necessary precautions would result in highly inaccurate solutions.

We have explored ways to address the condition of matrix $A^{(2)}$ in order to obtain reliable solutions for the particular case discussed here. First, the spacing among the measuring points of the UVP should be defined, minimizing the condition number of $A^{(2)}$. It was heuristically found that equally spaced velocity measurement points gave the best results. Second, the system should be solved using an appropriate method for solving ill-conditioned systems. Using a biconjugate gradient stabilized method proved to be enough for the present case, using preconditioners was explored without significant improvement of the results.

3.2. Measurement simultaneity

The UVP does not measure the velocity at each spatial point at the same exact time. The time lag between two measuring points, or channels as they are called in the UVP, is the time that takes the sound to travel the distance between them. Considering that Eq. (21) is evaluated at $t+\Delta t_{\text{lag}}$ a correction could be implemented. Here Δt_{lag} is the time that takes the sound to travel between the point considered and a reference point.

The correction implies adding a term $\omega\Delta t_{\text{lag}}$ when defining the $C_I^{(1)}$ and $C_R^{(1)}$, and $2\omega\Delta t_{\text{lag}}$ when defining $C_{I,B}^{(2)}$, $C_{R,B}^{(2)}$, $C_{I,F}^{(2)}$ and $C_{R,F}^{(2)}$ resulting in

$$C_I^{(1)} = k_0\left[iZ^{(1)}sin(\alpha)+Y^{(1)}cos(\alpha)\right]exp[-i(k_0\Delta x_m-\omega\Delta t\text{lag})]/2, \quad (59)$$

$$C_R^{(1)} = k_0\left[iZ^{(1)}sin(\alpha)-Y^{(1)}cos(\alpha)\right]exp[+i(k_0\Delta x_m+\omega\Delta t\text{lag})]/2, \quad (60)$$

$$C_{I,B}^{(2)} = +2k_0\left[Z_B^{(2)}sin(\alpha)-iY_B^{(2)}cos(\alpha)\right]exp(-i(2k_0\Delta x_m-2\omega\Delta t\text{lag}))/2, \quad (61)$$

$$C_{R,B}^{(2)} = -2k_0\left[Z_B^{(2)}sin(\alpha)+iY_B^{(2)}cos(\alpha)\right]exp(+i(2k_0\Delta x_m+2\omega\Delta t\text{lag}))/2, \quad (62)$$

$$C_{I,F}^{(2)} = -\kappa\left[Z_F^{(2)}sin(\alpha)-iY_F^{(2)}cos(\alpha)\right]exp(-i(\kappa\Delta x_m-2\omega\Delta t\text{lag}))/2, \quad (63)$$

$$C_{R,F}^{(2)} = +\kappa\left[Z_F^{(2)}sin(\alpha)+iY_F^{(2)}cos(\alpha)\right]exp(+i(\kappa\Delta x_m+2\omega\Delta t\text{lag}))/2. \quad (64)$$

Additionally, $A^{(1)}$, $b^{(1)}$, $A^{(2)}$, and $b^{(2)}$ need to be redefined, in this case $-C_I^{(1)*}\neq C_R^{(1)}$, $-C_{I,B}^{(2)*}\neq C_{R,B}^{(2)}$ and $-C_{I,F}^{(2)*}\neq C_{R,F}^{(2)}$ but the resulting matrices will still be Hermitian matrices. However, considering that the speed of sound in water is close to 1500 m/s and that the surface wave celerities are usually less than 2 m/s, the time correction would be in the order of 0.1%. Nevertheless, we implemented this correction and as it was expected that the correction did not introduce any significant change to the final solution.

3.3. Period determination

For cases where the first harmonic wave period was not exactly known, the measured data itself were used to determine it. The fundamental wave period was obtained minimizing

$$\sum_m \left| \frac{1}{T}\int_0^T v_r(x_m,z_m,t)exp\left(-\frac{i2\pi t}{T}\right) \right|. \quad (65)$$

This determination was implemented for both measuring systems, wave gages and UVP, and for all the tested cases the same fundamental periods were obtained for both systems.

3.4. Accuracy

The proposed method was first tested and verified using synthetic generated signals with excellent results. The effect of random noise was not addressed during this early testing stage in the understanding that an actual signal may present noise with a priori unknown characteristics. Furthermore, an actual signal may contain energy in the third or higher harmonics that would affect the overall performance of the method. It was therefore decided to assess the accuracy of the method directly using the measured data and comparing the results obtained using the four wave gages (Lin and Huang, 2004 method) and the UVP (proposed method).

As an objective way to evaluate the accuracy of the results the Signal to Residual Ratio (SRR) was defined. The SRR is the ratio between the energy of the signal E_{signal} and the energy of the residual E_{residual}, and it is measured in dB

$$\text{SRR} = 10\,log_{10}\left(\frac{E_{\text{signal}}}{E_{\text{residual}}}\right), \quad (66)$$

The residual was introduced in Eq. (21) and is defined as the difference between the fitted and measured signals. The SRR for the performed experiments was in the order of 15 dB when using the UVP measurements and of 10 dB when using the wave gage measurements, as discussed in Section 4, and presented in Table 1.

Table 1
Comparison of the decomposed wave amplitudes using four wave gages and Lin and Huang's (2004) method (WG-Lin), and four UVP channels and the proposed method (UVP). The global reflection coefficient K_R and the Signal to Residual Ratio (SSR) are also included.

Amplitude	Vertical wall		Impermeable beach		Permeable beach	
(cm)	WG-Lin	UVP	WG-Lin	UVP	WG-Lin	UVP
$a_I^{(1)}$	3.5	3.1	2.6	2.8	3.2	3.1
$a_R^{(1)}$	3.2	2.7	0.8	0.9	0.3	0.2
$b_{I,B}^{(2)}$	0.9	0.9	0.5	0.8	0.7	0.7
$b_{R,B}^{(2)}$	0.9	1.1	0.1	0.2	0.1	0.2
$a_{I,F}^{(2)}$	0.2	0.3	0.2	0.1	0.1	0.2
$a_{R,F}^{(2)}$	0.2	0.5	0.4	0.4	0.1	0.1
$K_R(\%)$	92	91	33	35	10	10
$SRR(dB)$	7.9	14.4	13.0	15.4	10.4	18.3

3.5. General procedure

The proposed method was implemented in our laboratory in the following way

1. The UVP was installed and all the geometrical characteristics were measured: distance between the sensor and the bottom of the flume, angle of the sensor with the vertical, and still water depth in the flume. The water temperature was also measured in order to compute the speed of sound.
2. The quantities x_m, z_m, $C_I^{(1)}$, $C_{I,B}^{(2)}$, and $C_{I,F}^{(2)}$ were computed for each UVP channel to be used. The condition number of $A^{(2)}$ was evaluated. If necessary the selected channels were modified and the sensor angle was adjusted. The period of the first harmonic had to be known at this point, if it was unknown the maximization of the expression (65) was used to obtain it.
3. The velocity data were collected with the UVP. In order to facilitate the post-processing of the data, the data collection duration was selected as an integer number of wave periods and the total number of samples to be a power of 2.
4. The quantities $\hat{v}_r^{(1)}$ and $\hat{v}_r^{(2)}$ were computed using Eq. (25) for each selected channel.
5. The systems (34) and (50) were solved using a biconjugate gradients stabilized method and each harmonic amplitude was computed using Eqs. (37) and (53).

4. Experiments, results, and discussion

Three experiments are presented in this section, representing three different wave reflection conditions in the flume. These experiments allowed us to explore the advantages of the proposed method, and to compare the proposed method against the one proposed by Lin and Huang (2004). As a side product, the experiments served as a way of testing of Lin and Huang's (2004) method against actual wave data. It should be pointed out here that Lin and Huang only validated their method against synthetically generated signals with white noise added, without considering the possible presence of higher harmonics in the signal.

Each experiment reported here was both measured with the UVP and with four wave gages. The experiments were performed in a wave flume at the Instituto de Mecánica de los Fluidos e Ingeniería Ambiental (IMFIA). The wave flume working zone is 15.8 m long, 0.5 m wide, and 0.76 m high. The side walls are made of glass. At the time of the measurements the flume had a wood false bottom installed for other proposes. The false bottom starts 1.2 m away from the wave maker with a 2.8 m long and 0.15 m high ramp. After the ramp, the false bottom continues horizontally for the remaining 11.8 m of the flume. An electrical motor imposes a sinusoidal movement to the wave maker which allows for both flap and piston-type wave generation. A permeable filter located in front of the wave maker minimizes the energy of waves reflected on the wave maker. The amplitude of the wave maker excursion was set to 0.095 m. The water depth h was 32 cm and the period T of the first harmonic was 1.91 s for all the experiments.

Three different reflection conditions were studied introducing different "beach" types at the end of the flume opposite to the wave maker. First, a vertical wall, which should approximate total reflection conditions. Second, an impermeable beach with a 17° angle with the horizontal, which should approximate partial reflection conditions. Finally, a permeable beach that should have only very minor reflection.

The distance between the UVP sensor and the flume false bottom was 15.5 cm, and the sensor was placed horizontally facing the waves.

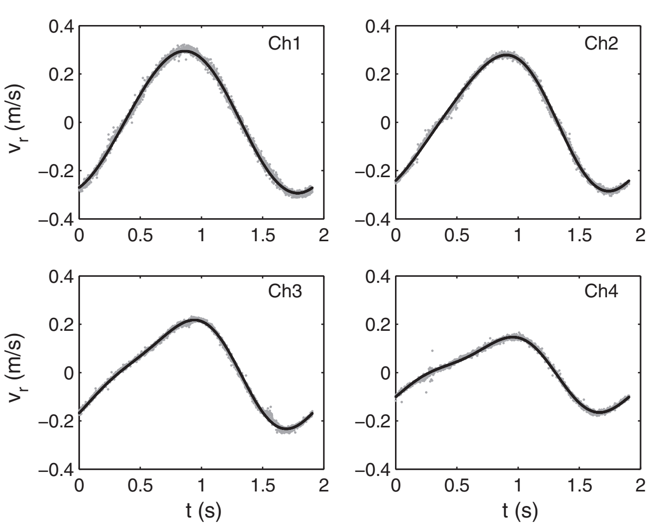

Fig. 2. Measured velocities for each of the four selected UVP channels overlapped over one oscillation cycle (gray dots), and reconstructed velocity obtained after the wave decomposition using the proposed method (black line). Experimental conditions: $h = 0.32$ m, $T = 1.91$ s, vertical wall at the flume end.

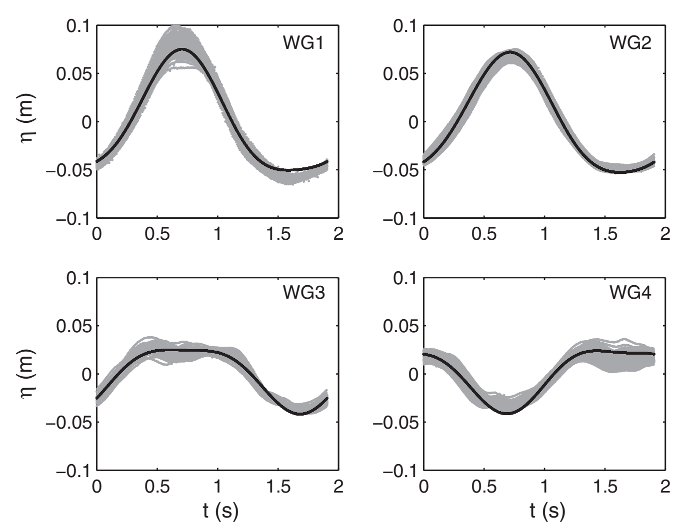

Fig. 3. Measured water surface elevation for each of the four wave gages overlapped over one oscillation cycle (gray dots) and reconstructed velocity obtained after the wave decomposition using Lin and Huang's (2004) method (black line). Experimental conditions: $h = 0.32$ m, $T = 1.91$ s, vertical wall at the flume end.

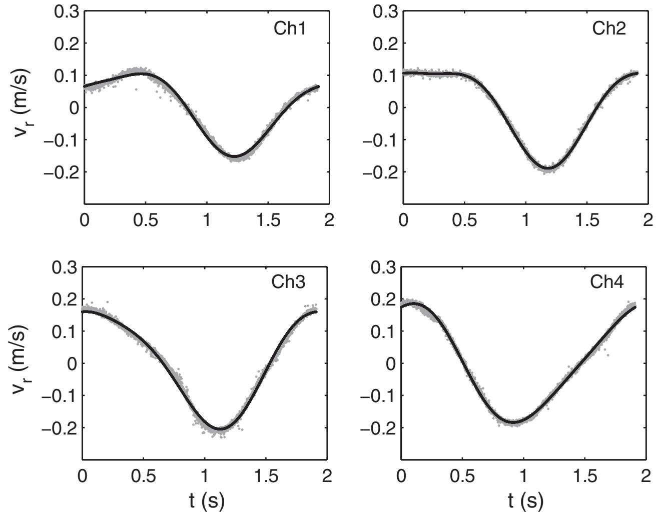

Fig. 4. Measured velocities for each of the four selected UVP channels overlapped over one oscillation cycle (gray dots), and reconstructed velocity obtained after the wave decomposition using the proposed method (black line). Experimental conditions: $h=0.32$ m, $T=1.91$ s, inclined table at the flume end.

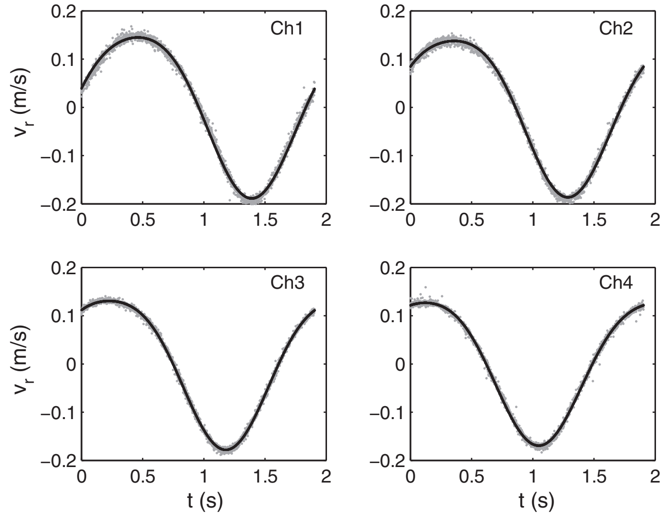

Fig. 6. Measured velocities for each of the four selected UVP channels overlapped over one oscillation cycle (gray dots), and reconstructed velocity obtained after the wave decomposition using the proposed method (black line). Experimental conditions: $h=0.32$ m, $T=1.91$ s, permeable beach at the flume end.

The developed method allows for any orientation of the sensor. However, given the experimental conditions the sensor was positioned horizontally. The distance between each channel of the UVP was 2.9 mm and velocity measurements were obtained for 344 channels, covering a distance of approximately 70 cm. The distances from the first used channel to the second, third, and fourth used channels were 19.4 cm, 38.6 cm and 58.0 cm, respectively. The sampling rate of the UVP was 17 Hz and data were collected for approximately 2 min.

Additionally, four resistive wave gages were installed. The wave gages were made in our institute and were calibrated before and after the experiments. The wave gage design follows the design proposed by Guaraglia (1986), which includes a compensation method to minimize the drift of the measurements associated with water conductivity changes. The distances from the first wave gage to the second, third and fourth wave gages were 0.40 m, 0.73 m and 1.23 m, respectively. The same sampling rate and recording time of the UVP were used.

Figs. 2 to 7 show the entire recorded data collapsed over one wave cycle for the four UVP selected channels and for the four wave gages for each of the three described experiments. The measured data are shown using gray dots. Very little dispersion of the measurements is observed for the UVP measurements, confirming the reduced noise level of the UVP velocity measurements. Additionally the UVP results assure that a steady wave field was present in the flume during the experiments, which was confirmed by direct observation during the experiments. The wave gage signals present a somehow larger dispersion. This could be thought to be originated by the presence of capillary and transverse waves in the flume, or to a higher noise level of the wave gage system compared to the UVP's. However, a careful study of the data set indicates that the small but unavoidable variations of the waves generated within the flume are the reason for the observed scatter. These variations are the result of the interaction of the reflected waves with the wave-maker, which manifest in a much stronger way on the water surface than they do inside the water column. This suggests that the proposed water

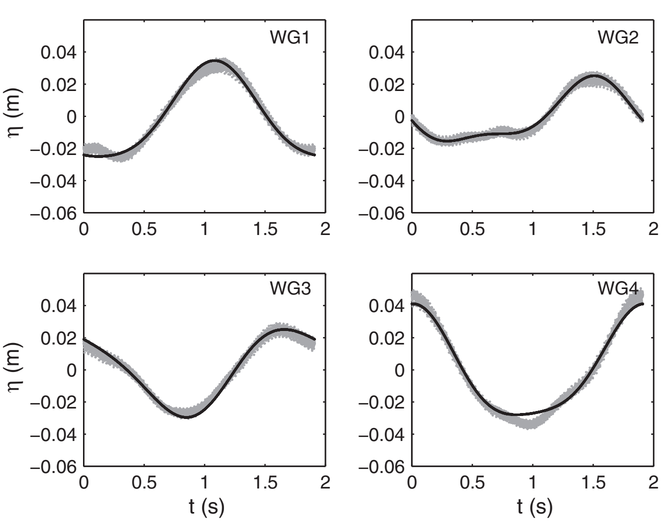

Fig. 5. Measured water surface elevation for each of the four wave gages overlapped over one oscillation cycle (gray dots) and reconstructed velocity obtained after the wave decomposition using Lin and Huang's (2004) method (black line). Experimental conditions: $h=0.32$ m, $T=1.91$ s, inclined table at the flume end.

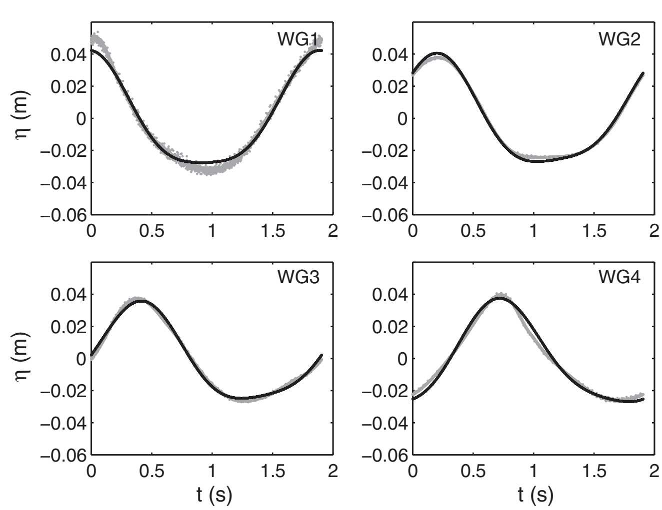

Fig. 7. Measured water surface elevation for each of the four wave gages overlapped over one oscillation cycle (gray dots) and reconstructed velocity obtained after the wave decomposition using Lin and Huang's (2004) method (black line). Experimental conditions: $h=0.32$ m, $T=1.91$ s, permeable beach at the flume end.

velocity based method may be more robust than the existing surface elevation based methods.

In Figs. 2 to 7, the signal recovered from the harmonic analysis is shown with a black line for each of the UVP channels and each of the wave gages. The agreement of the recovered signal with the measurements is clearly superior in the case of the UVP. The wave gage data suggests the presence of higher harmonics in the wave field which are not observed in the UVP measurements. This is due to the fact that short waves would be associated with water motions closer to the water surface, that are not captured by the UVP which was located at mid water depth. Additionally, the results may also suggest that the second order theory used here may give a better representation of the velocity field inside the water column than it does on the water surface. In this regard, Dean (1972) found during the evaluation of water wave theories that the Airy theory performed significantly better over a wider range of wave conditions if it was evaluated against water column velocity data than if it was evaluated against free surface data. Finally, it should be mentioned that the surface elevation is obtained from imposing the dynamic boundary condition at the water surface (Eqs. (11) and (12)), which is a nonlinear equation, and allows for nonlinear interactions among different order terms, as was the case of the terms presented in Eqs. (14) and (15). Meanwhile the velocity field is obtained from the direct spatial derivation of the velocity potential (Eqs. (19) and (20)) which is a linear equation and therefore non-linear interactions are not possible.

Table 1 summarizes the computed wave amplitudes for the incident and reflected the first and second harmonics for each of the three experiments. The results were computed from water elevation measurements applying Lin and Huang's (2004) method, and from velocity measurements applying the proposed method. The SRR and a global reflection coefficient K_R are included in Table 1. The global reflection coefficient in wavenumber space and in terms of the surface wave amplitudes is defined as

$$K_R = \left[\frac{a_R^{(1)2} + b_{R,B}^{(2)2} + a_{R,F}^{(2)2}}{a_I^{(1)2} + b_{I,B}^{(2)2} + a_{I,F}^{(2)2}}\right]^{1/2}. \tag{67}$$

Both methods give similar results, but the proposed method gives lower SRR values for all reflection conditions, better capturing the behavior of the measured signal as discussed before. It should be noticed that the distance between the first and the last wave gage was about 1.20 m, while the distance between the first and last used UVP channel was less than 0.7 m. This may allow for the accurate characterization of the wave field using information obtained over a limited extension along the wave flume and can be used to obtain “local” descriptions of the wave field in configurations where the spatial variations of the wave field are expected, as is the case of waves propagating over a mild slope bottom.

5. Summary and future work

We have introduced a novel method to determine the decomposition of incident and reflected regular waves in a wave flume including the discrimination of the second order free and bound harmonics. The method uses the velocity measurements inside the water column, which showed to be more robust and easier to implement than the traditional wave gage based methods. The proposed method was evaluated over a wide range of reflection conditions with excellent results. Since ultrasonic instruments do not need calibration the tedious wave gage calibration routine is completely avoided. Furthermore, the interference with the wave motion is greatly reduced since only one sensor has to be inserted into the flume to obtain the wave field characterization. Finally, since velocity measurements over only a fraction of the first harmonic wavelength are necessary, the proposed method allows for the “local” characterization of the wave field.

We foresee several extensions of the presented work. As the water velocity is directly measured the extension of the proposed method to the study of waves in the presence of a superimposed current would not require any additional set-up. Additionally, it is possible to extend the method to the three dimensional characterization of the incident and reflected waves in wave basins using two perpendicular velocity profilers. Finally, it should be mentioned that all the available methods used to decompose the wave field in a wave flume relay on the application of the dispersion equation to relate frequencies and wavelengths. In the proposed method the velocity profiles are measured over both time and space with excellent resolution, eventually it would be possible to directly relate frequency and wavelength by directly studying the 2D (frequency-wavelength) Fourier transform of the velocity profiles. This would require measuring velocity profiles over at least two first harmonic wavelengths, which was not possible to implement in a practical way in the present time, due to limitations of the available instrumentation. We are planning to continue working on these extensions to the proposed method in the near future.

Acknowledgments

This work was done under the grant PR_FMV_2009_1_1890 from the Agencia Nacional de Investigación e Innovación, Uruguay. This support is greatly appreciated. The authors would like to thank Valentina Groposo for her help during the experiments, and the IMFIA machine shop staff (Daniel Barboza and Ricardo Zouko) for their help with the experimental set-up.

References

Baquerizo Azofra, A., 1995. Reflexión del oleaje en playas. Métodos de evaluación y de predicción. Ph.D. thesis, Universidad de Cantabria, Santander.
Biesel, F., Suquet, F., 1951. Les appareils générateurs de houle en laboratoire. La Houille Blanche 5, 723–737.
Brandwood, D.H., 1983. A complex gradient operator and its application in adaptive array theory. Microwaves, Optics and Antennas, IEE Proceedings H 130 (1), 11–16.
Dean, R.G., 1972. Evaluation and development of water wave theories for engineering application. Presentation of Research Results. : Technical Report 14, volume I. Coastal and Oceanographic Engineering Laboratory, University of Florida, Gainesville.
Fontanet, P., 1961. Théorie de la génération de la houle cylindrique par un batteur plan (2e ordre d'approximation). La Houille Blanche 1, 23–31.
Goda, Y., Suzuki, Y., 1976. Estimation of incident and reflected waves in random wave experiments. Proceedings of 15th ICCE. ASCE, pp. 828–845.
Guaraglia, D., 1986. Desarrollo de un sistema para la medición de olas en modelos hidráulicos. XXI Congreso Latinoamericano de Hidráulica, San Pablo, pp. 281–292.
Hancock, M.J., 2005. Generation of sand bars under surface waves. Ph.D. thesis, Massachusetts Institute of Technology, Dept. of Civil and Environmental Engineering.
Havelock, T.H., 1929. Forced surface-waves on water. Philosophical Magazine 8, 569–576.
Hughes, S.A., 1993. Laboratory wave reflection analysis using co-located gages. Coastal Engineering 20 (3–4), 223–247.
Lin, C., Huang, C., 2004. Decomposition of incident and reflected higher harmonic waves using four wave gauges. Coastal Engineering 51 (5–6), 395–406.
Madsen, O.S., 1971. On the generation of long waves. Journal of Geophysical Research 76 (36), 8672–8683.
Mansard, E., Funke, E., 1980. The measurement of incident and reflected spectra using a least square method. Proceedings of the 17th International Conference on Coastal Engineering, vol. 2, pp. 154–172.
Met-Flow, 2002. UVP Monitor User's Guide. Met-Flow SA, Lausanne.
Pedocchi, F., García, M.H., in press. Acoustic measurement of suspended sediment concentration profiles in an oscillatory boundary layer. Continental Shelf Research, http://dx.doi.org/10.1016/j.csr.2011.05.013.
Sulisz, W., Hudspeth, R., 1993. Complete second-order solution for water waves generated in wave flumes. Journal of Fluids and Structures 7 (3), 253–268.